Copyright WILEY-VCH Verlag GmbH & Co. KGaA,69469 Weinheim,Germany,2012.

NANO MICRO small

Supporting Information

for *Small*,DOI: 10.1002/smll.201200864

From Bare Metal Powders to Colloidally Stable TCO Dispersions and Transparent Nanoporous Conducting Metal Oxide Thin Films

*Engelbert Redel, Chen Huai, Ömer Dag, Srebri Petrov, Paul G. O'Brien, Michael G. Helander, Jacek Mlynarski, and Geoffrey A. Ozin**

Submitted to small

Supporting Material Information

From Bare Metal Powders to Colloidally Stable TCO Dispersions and Transparent Nanoporous Conducting Metal Oxide Thin Films.**

*Engelbert Redel[a], Chen Huai[a], Ömer Dag[b], Srebri Petrov[a], PaulG. O'Brien[a], Michael G. Helander[c], Jacek Mylnarski[a] and Geoffrey A. Ozin[a]**

[a] *Materials Chemistry and Nanochemistry Research Group, Center for Inorganic and Polymeric Nanomaterials, Chemistry Department, 80 St.George Street, University of Toronto, Toronto, M5S 3H6, Ontario, Canada*
[b] *Department of Chemistry, Bilkent University, 06800, Ankara, Turkey*
[c] *Faculty of Applied Science & Engineering, Wallberg Building, 184 College Street, Suite 140, Toronto, M5S 3E4, Ontario, Canada*

E-mail: gozin@chem.utoronto.ca

Experimental Section

Synthesis details:

SnO_2, In_2O_3, ITO (≡In_2O_3:Sn), ATO (≡SnO_2:Sb) and ZTO (≡SnO_2:Zn) were synthesized by simple dissolution of 1-3 g of the elemental metal powder of Sn, In, Sb and Zn (ASP ≤ 10 µm, mesh 200 and 325), dispersed in 5 ml of de-ionised H_2O (0.056 µS/cm) followed by the addition of 8 mL HCl (Hydrochloric Acid. 37 wt.%) at 0°C and after ≈ 20 to max. 30 mins *the slow and drop wise addition* of 10-25 mL H_2O_2 (30%. p.a.) under nitrogen by cooling the reaction mixture with an ice-bath due to an exothermic dissolution/oxidation process, followed by further stirring of the mixture for 12-18 h under air/nitrogen. Addition of HCl causes the complete dissolution of the native metal oxide layer of the respective metal powder(s) and causes the metal powder(s) to agglomerate into a compact metal piece, see pictures below.

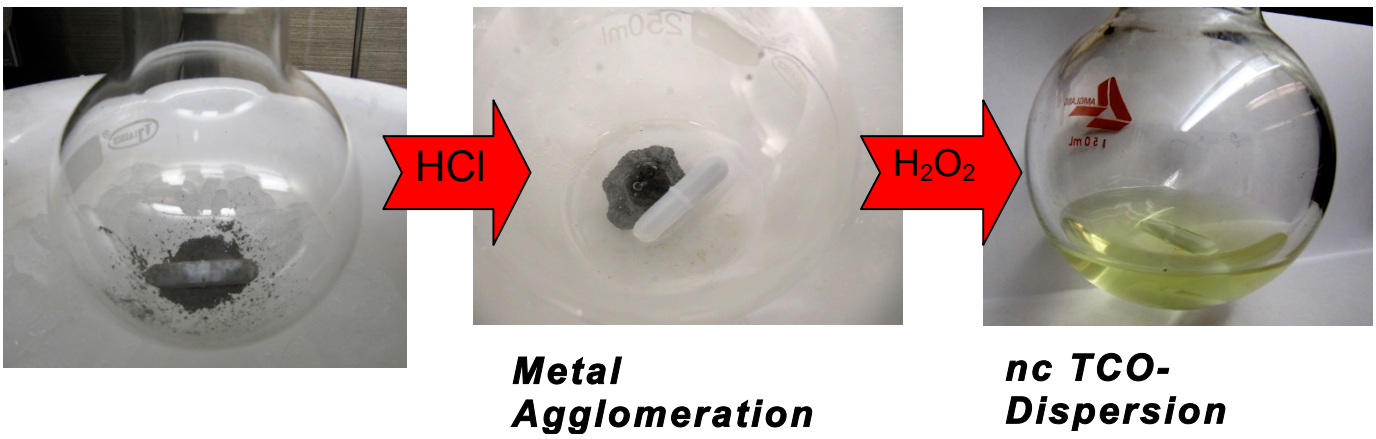

The synthesis must be performed in a well-ventilated fume-hood; addition of H_2O_2 (p.a. 30%) must be carried out *slowly and drop wise*, where permanent cooling is needed during the addition and reaction/ dissolution processes. The reaction vessel (2 neck round-bottom flask) 250 or 500 mL should be never closed too tightly. Final stirring of the reaction mixture, at RT, overnight leads for example to a light-yellow to yellow In_2O_3 dispersion, a transparent-milky SnO_2 dispersion and a blue-grey ATO (≡ SnO_2:Sb) dispersion which precipitates quickly due to larger particles, see Figure below. The dispersions were stored in plastic bottles at 4°C and the bottle-caps have additionally a hole in them. Dopants were introduced by weighing metal powders according to their molar ratios to obtain the desired TCO NP products.

TCOs Dispersions:

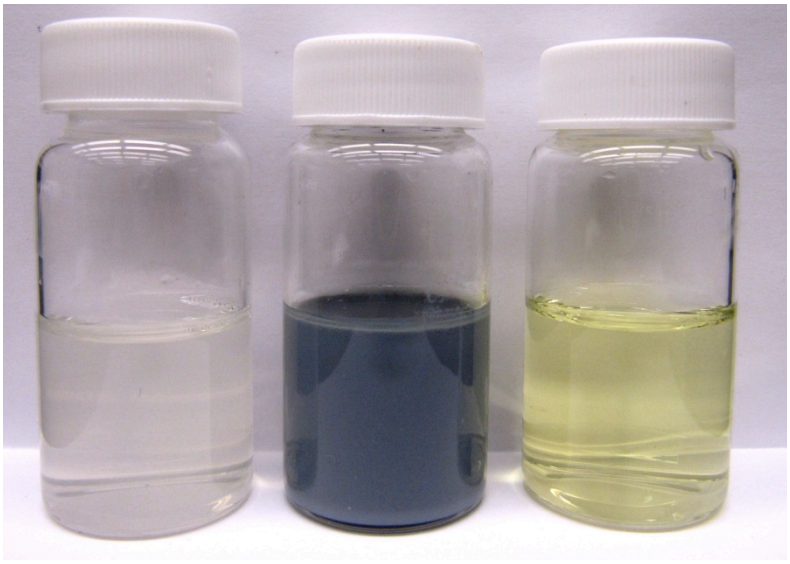

SnO_2 **ATO (≡ SnO_2:Sb)** **In_2O_3**

The resulting aqueous metal oxide dispersions were filtered through a 0.7 µm Titan 2 HPLC Filter Amber (GMF Membrane) and mixed with 2 to 15 wt.% polyethyleneglycol (PEG), MW: 20.000 before spin-coating on Si wafers. Spin coating of the TCO NP thin films was performed on a Lauriel single wafer spin coater (Model WS-400A-6NPP/LITE) at 2500-6000 rpm, 25-60 acceleration for 20-40 sec. The addition of PEG was performed to improve NP adhesion to the substrate and to ensure porosity and good film quality; PEG undergoes complete carbonization upon calcination at 450°C for 15-20 min.

Powder X-ray Diffraction:

The phase composition, lattice parameters and mean crystallite size of the films (annealed at 450°C for 15-20 mins in air) were analyzed by powder X-ray diffraction (XRD) using a Siemens D5000 diffractometer and Cu-K_α line as the X-ray source with step scan mode (step size, ss = 0.02°, time per step, t = 2.0 s) in the range of 20–65° 2θ. Phase identification was done using Eva 8.0™/Search-Match™ routine with PDF-2/2001. The Rietveld refinement was carried out with Bruker AXS general profile fitting software Topas™ v. 2.1.

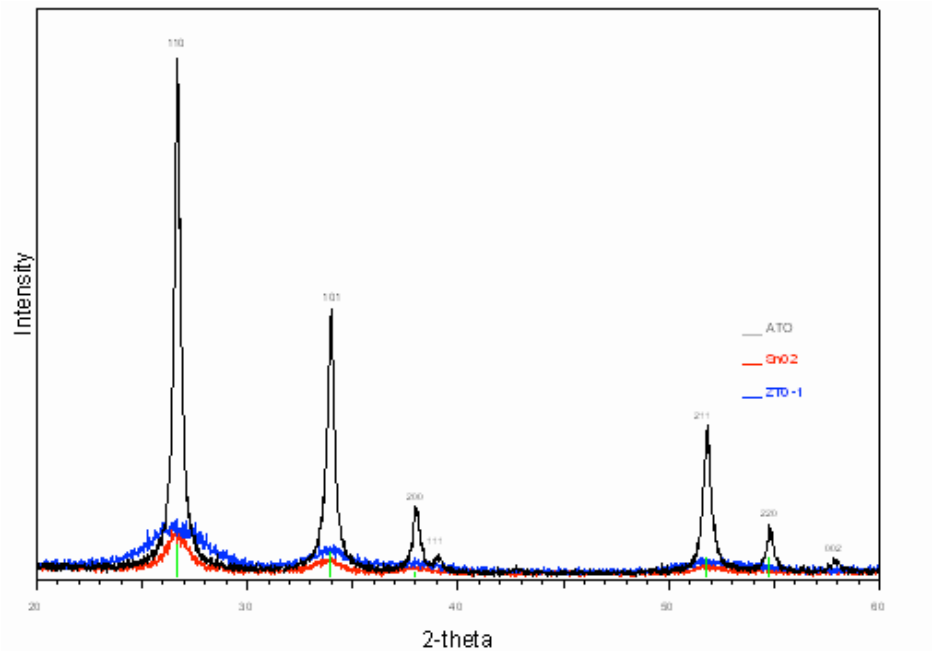

Figure S1: PXRD patterns of calcined TCOs thin films with SnO_2 – $(Sn,Sb,Zn)O_2$ composition. All of these TCO's have SnO_2 (Cassiterite) structure being solid solutions.

Table S1: Data for SnO_2 and ATO ≡ $(Sn.Sb)O_2$ thin films

Tetragonal lattice, SG $P4_2/mnm$ (136)				
Composition	Sn : Sb ratio	a, Å	c, Å	L_0, nm
SnO_2	-	4.7302(4)	3.1850(3)	9(2)
$(Sn,Sb)O_2$	25 : 2.3	4.7315(3)	3.1853(3)	18(3)

*a and c(Å) = lattice parameter in (Å)
* L_0 = mean particle size determined by PXRD method.

Table S2: Data for In_2O_3 and ITO ≡ $(In.Sn)_2O_3$ thin films

Sample	In : Sn ratio (mmol)	a, Å	L_0, nm
In_2O_3	-	10.1184(19)	14.2(5)
D1	26 : 1.3	10.1195(5)	20.6(4)
D2	26 : 2.6	10.1370(4)	33(3)
D3	26 : 3.9	10.1236(3)	20.2(3)
D4	26 : 5.2	10.1164(3)	16.3(6)

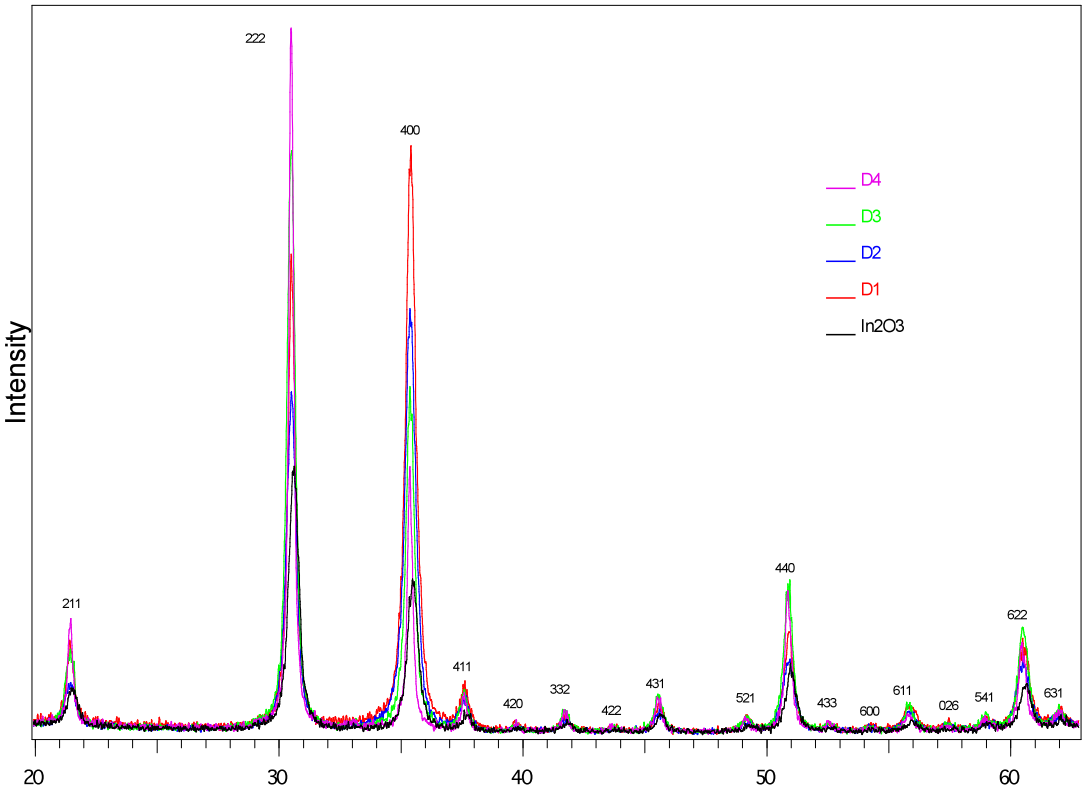

FigureS2a: PXRD patterns of calcined ITO thin films with $(In,Sn)_2O_3$ solid solution compositions.

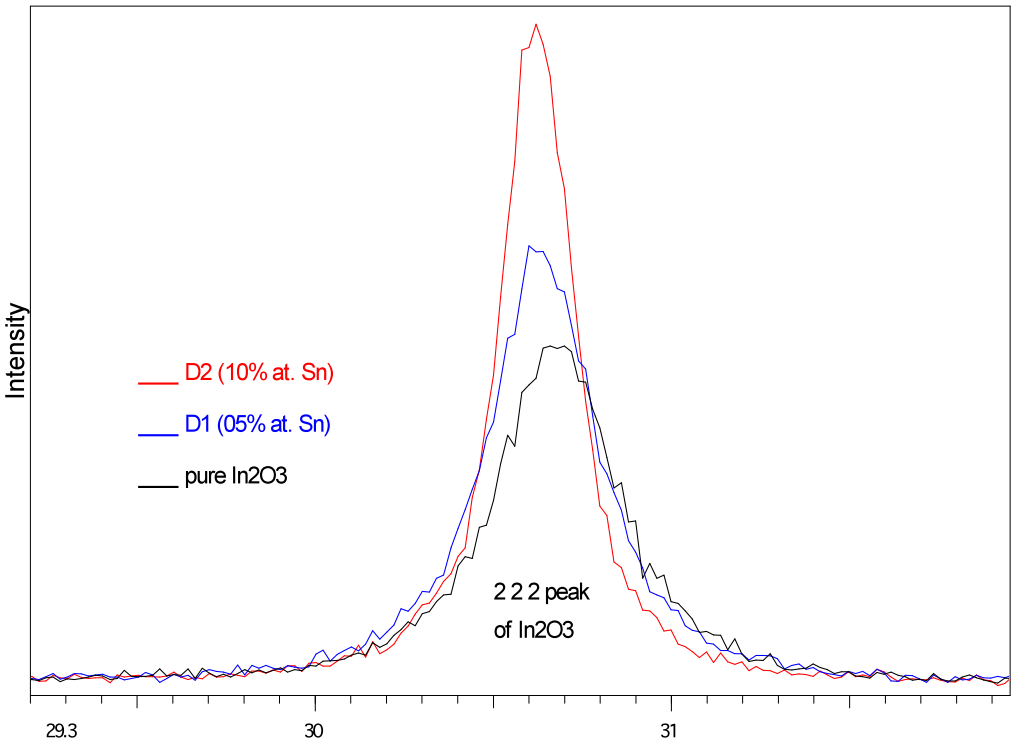

Figure S2b: PXRD patterns of calcined TCO NP thin films In_2O_3, D1 and D2 (inset; magnification of the chosen peak [222]; observed lattice parameter shift due to lattice enlargement based on an increase of the Sn doping-level.)

Cryo-STEM, HRTEM and SEM:

Examples of High-resolution scanning transmission electron microscopy (HR-STEM) were performed on a Hitachi HD-2000 in the Z-contrast mode at an accelerating voltage of 200 kV, emission current of 30-50μA. HR-TEM (high-resolution transmission electron microscopy) measurements were performed on a TITAN (FEI) at an accelerating voltage of 300 kV.

The FFT and inverse FFT analysis of a selected area was performed using DigitalMicrograph(TM) Demo 3.6.5 GMS1 software. The lattice fringes in the images and diffraction spots from the FFT of a selected area gave the lattice parameters of the metal oxide.

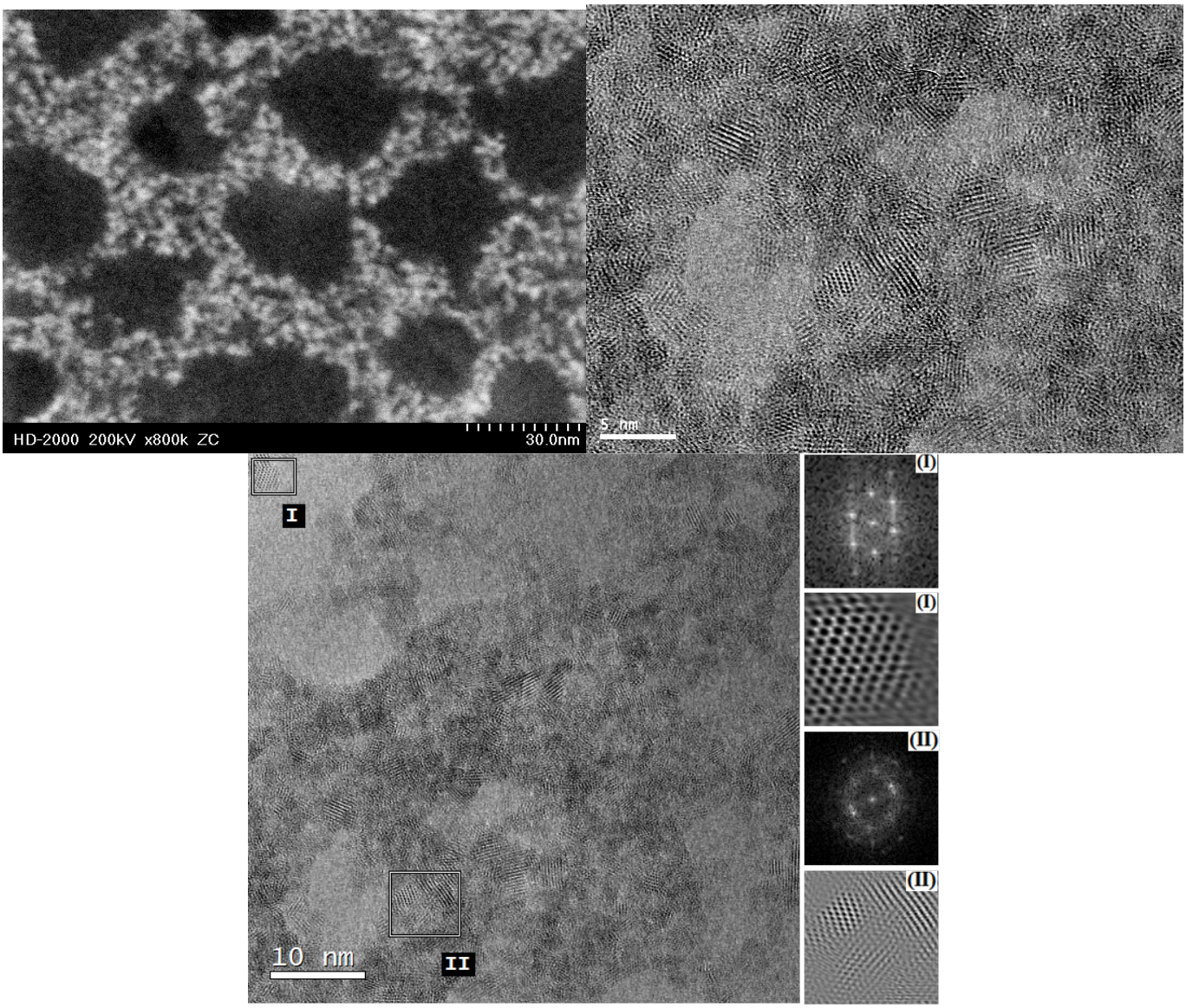

Figure S3: Cryo-STEM and HR-TEM images of SnO_2 NPs from $H_2O/HCl/H_2O_2$ dispersion. HR-TEM images of SnO_2 showing in the right column the FFT and inverse FFT of regions I and II in the TEM image. The lattice fringes (spacing 0.335 nm and 0.264 nm), observed in the HR-TEM images, are ascribed to the [110] and [200] planes of Rutile SnO_2 (Cassiterite) and are consistent with the PXRD results

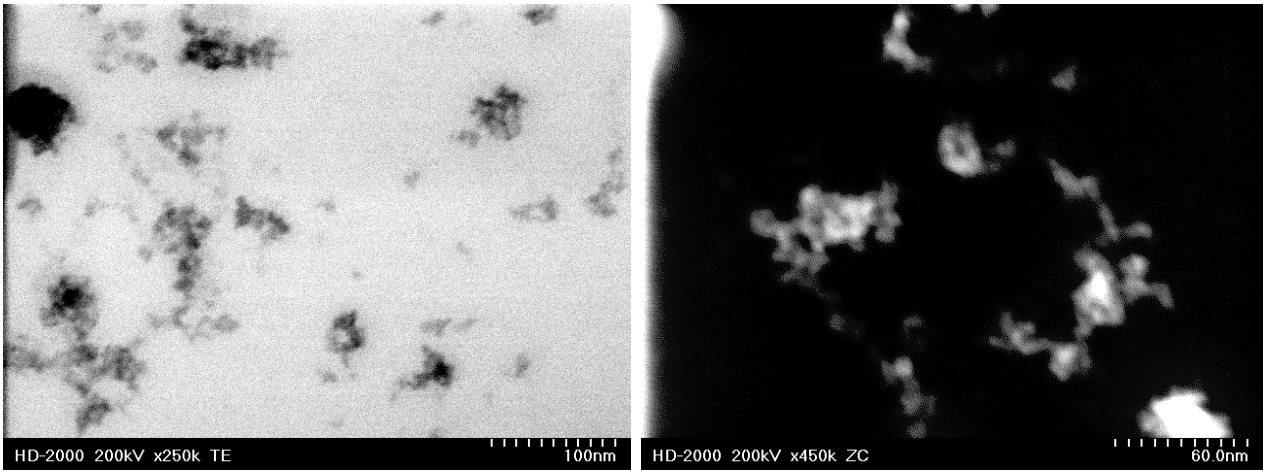

Figure S4: TEM and STEM images of ATO (≡ SnO_2:Sb) NPs from H_2O/HCl/H_2O_2 dispersion.

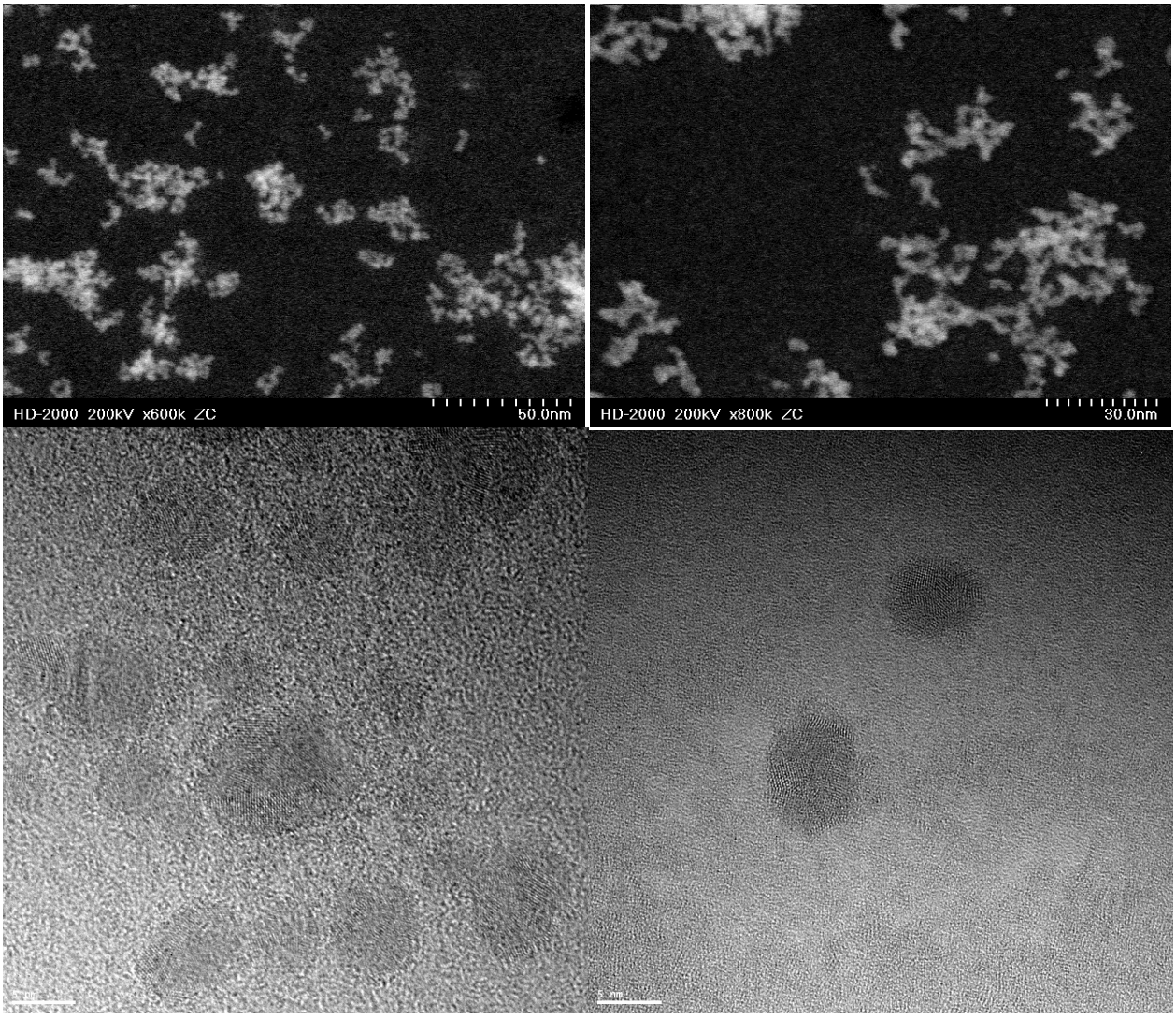

Figure S5: Cryo-STEM and HRTEM images of In_2O_3 NPs from H_2O/HCl/H_2O_2 dispersion.

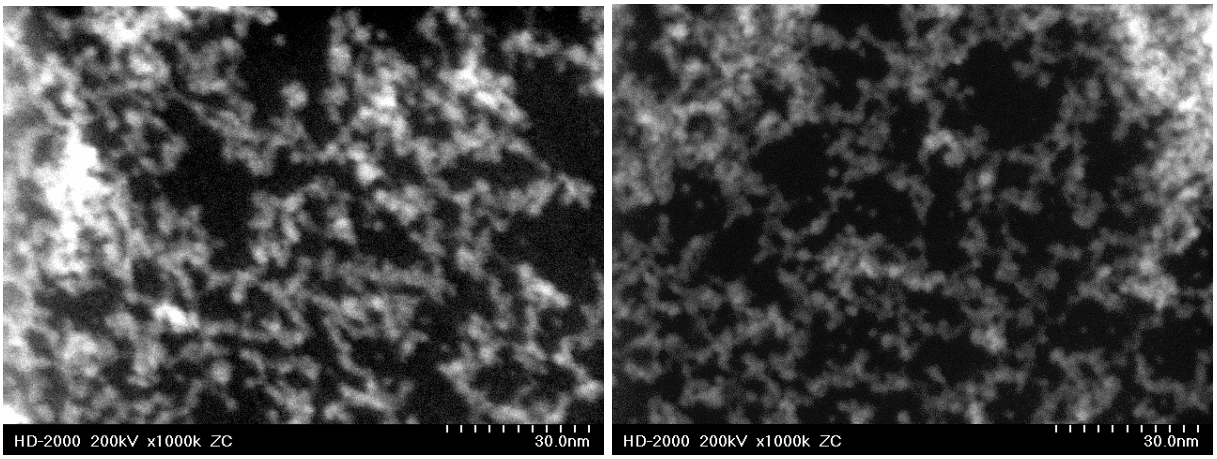

Figure S6: Cryo-STEM and STEM images of ZTO (≡ SnO_2:Zn) NPs from H_2O/HCl/H_2O_2 dispersion.

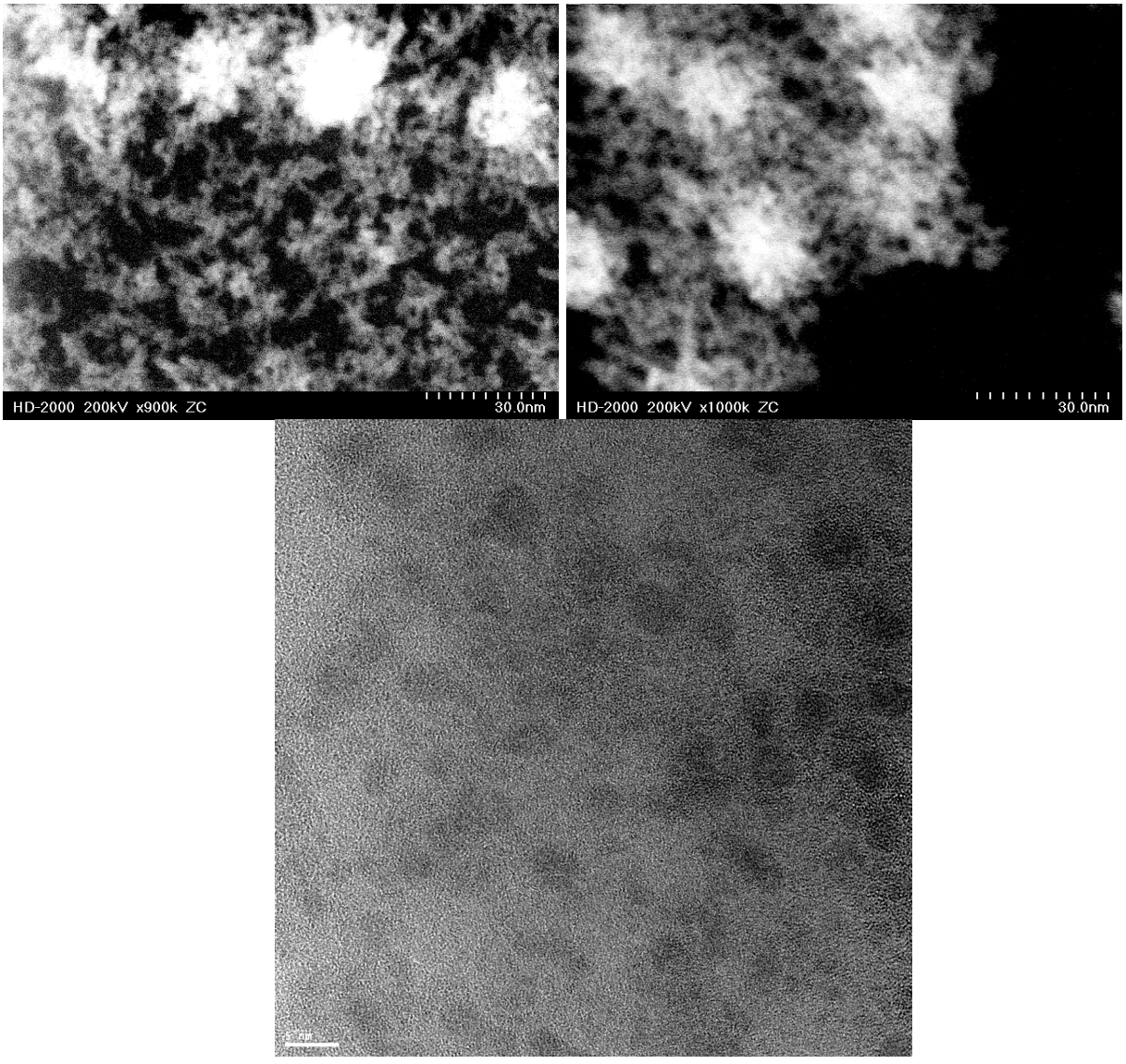

Figure S7: Cryo-STEM and HRTEM images of ITO (≡ In_2O_3:Sn) NPs from H_2O/HCl/H_2O_2 dispersion.

High-resolution scanning transmission electron microscopy (HR-STEM) and EDX spectroscopy (elemental mapping) were performed on a Hitachi HD-2000 in the Z-contrast mode at an accelerating voltage of 200 kV and emission current of 30-50µA. Due to signal collecting intensities, chosen agglomerates are yielding much better signal intensities rather than single particles, showing chlorine (Cl) located next to tin (Sn) and oxygen (O) ≡ SnO_2.

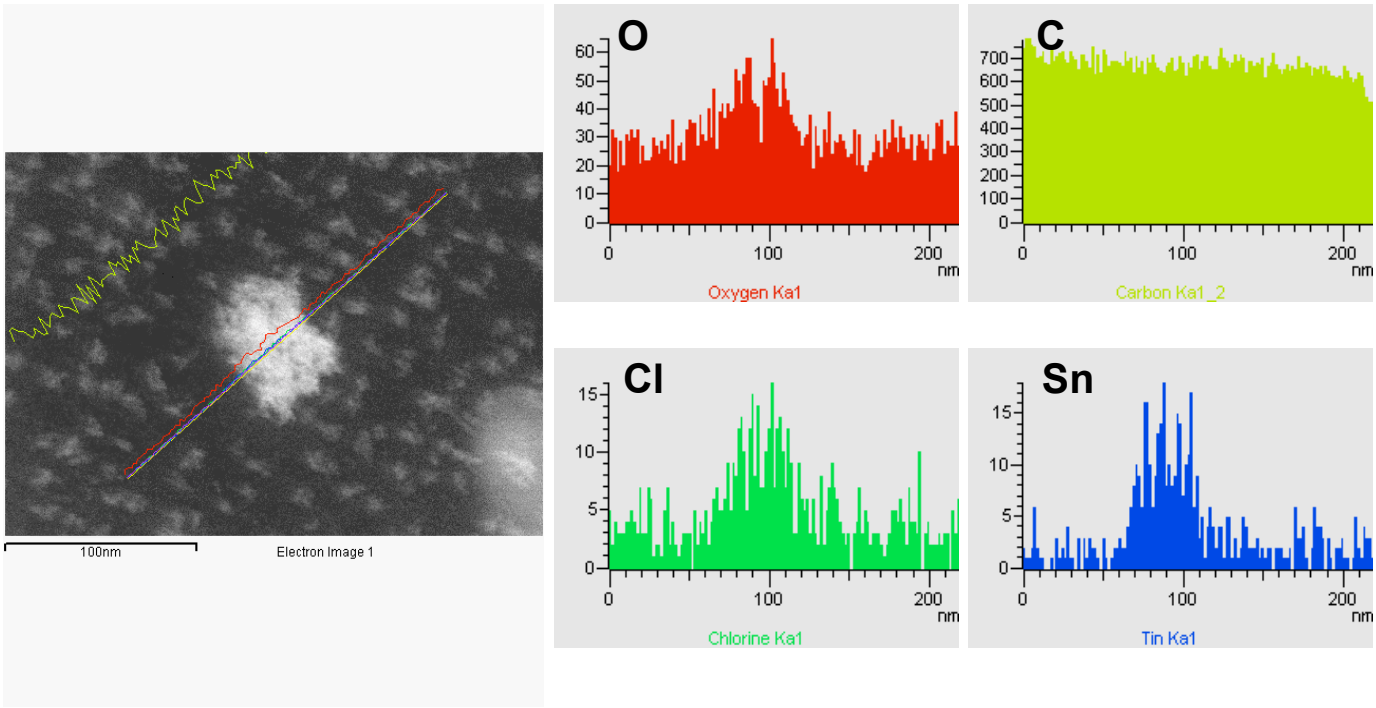

Figure S8: STEM analysis and EDX mapping of SnO_2 NPs from $H_2O/HCl/H_2O_2$ dispersion. (Signal intensities of Sn, O and Cl shown and source of C-signal ≡ grid background).

Scanning electron microscopy (SEM) cross-sectional images were obtained using a Hitachi S-5200 operating at 1-5 kV or at 30 kV for TCO NP films on silicon substrates. All the SEM cross-sections, Fig.S9-S13 have been recorded from films annealed at 450°C for 15-20 mins in air.

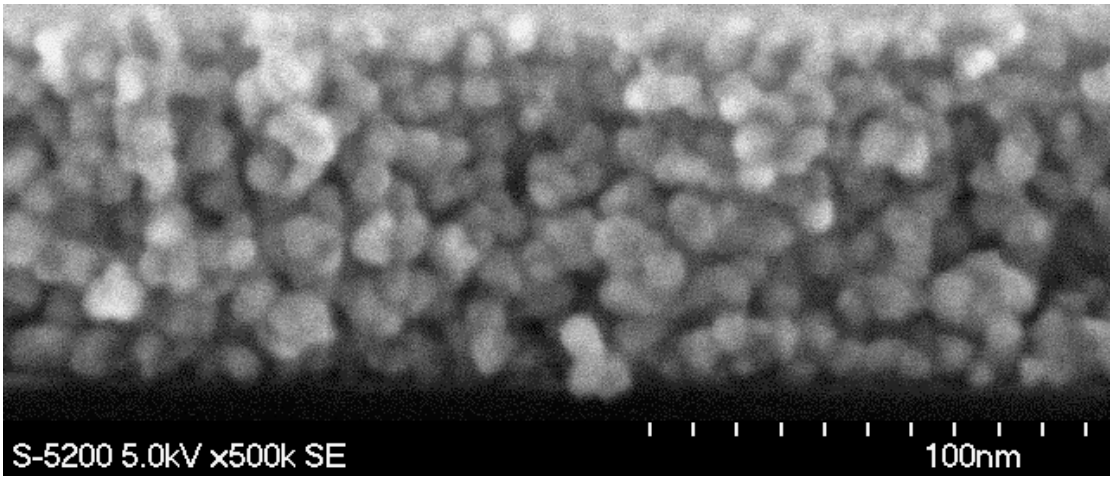

Figure S9: Example of a nanoporous SnO_2 thin film.

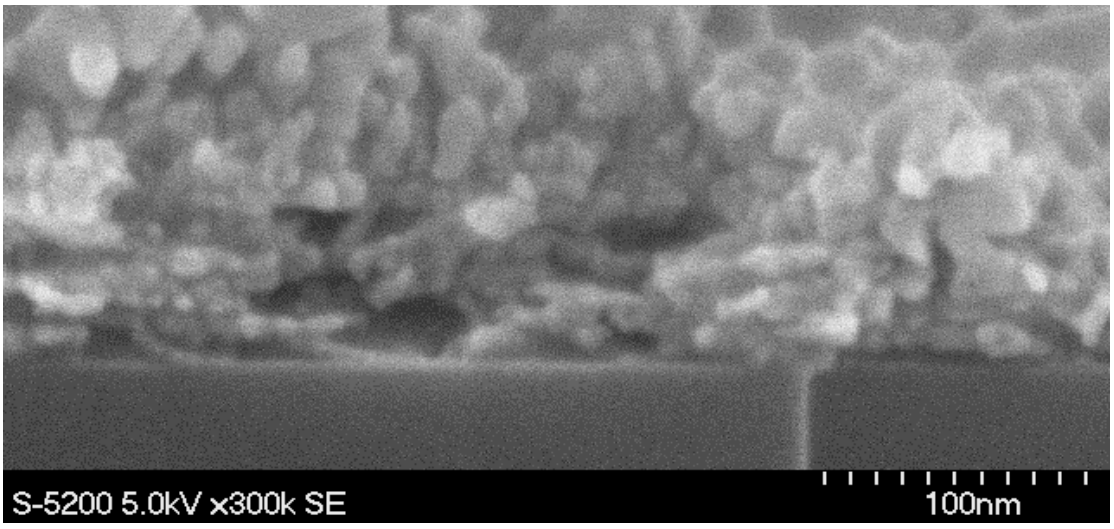

Figure S10: Example of a nanoporous In_2O_3 thin film.

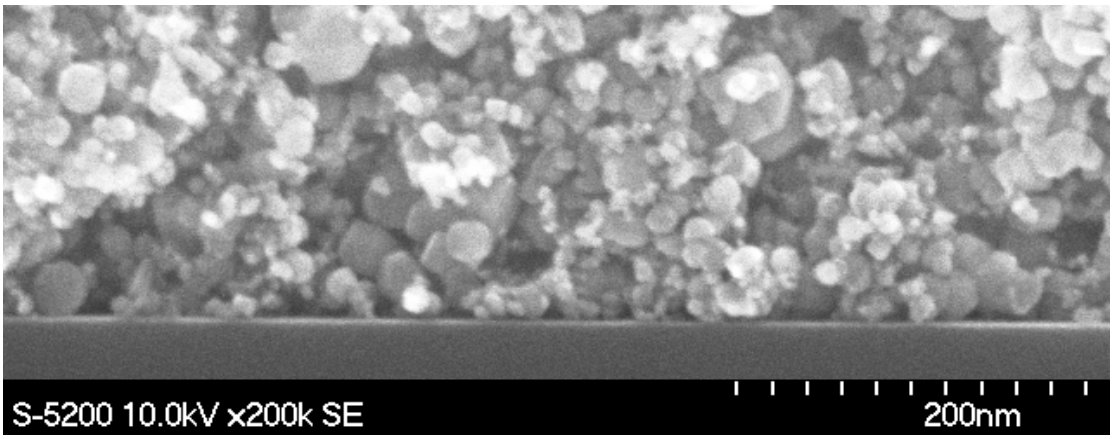

Figure S11: Example of a nanoporous ATO (≡ SnO_2:Sb) thin film.

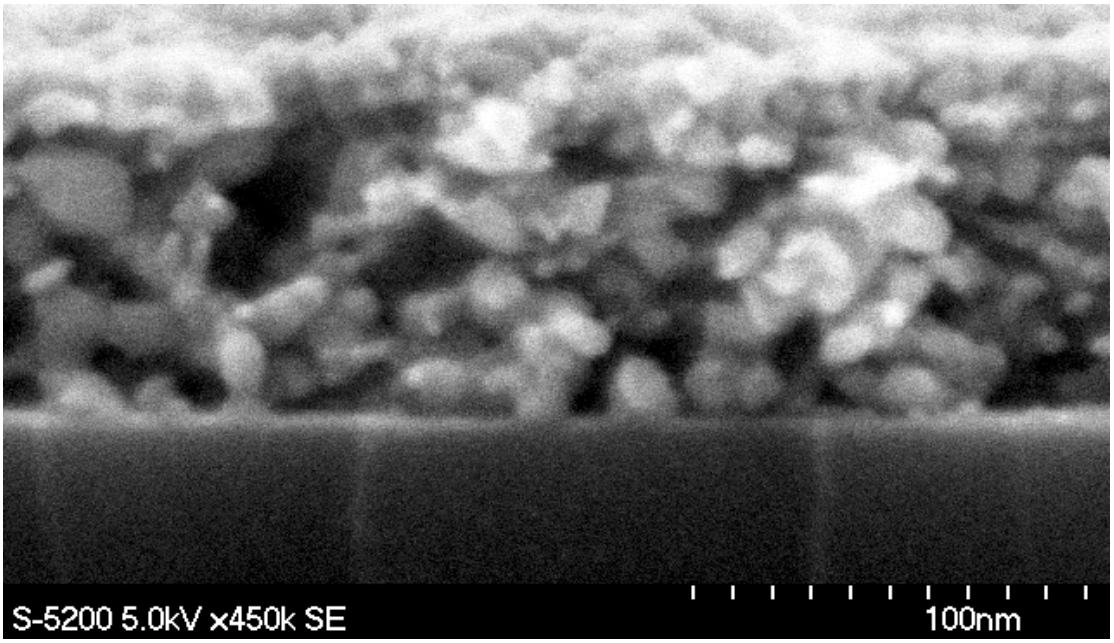

Figure S12: Example of a nanoporous ITO (≡ In_2O_3:Sn) thin film.

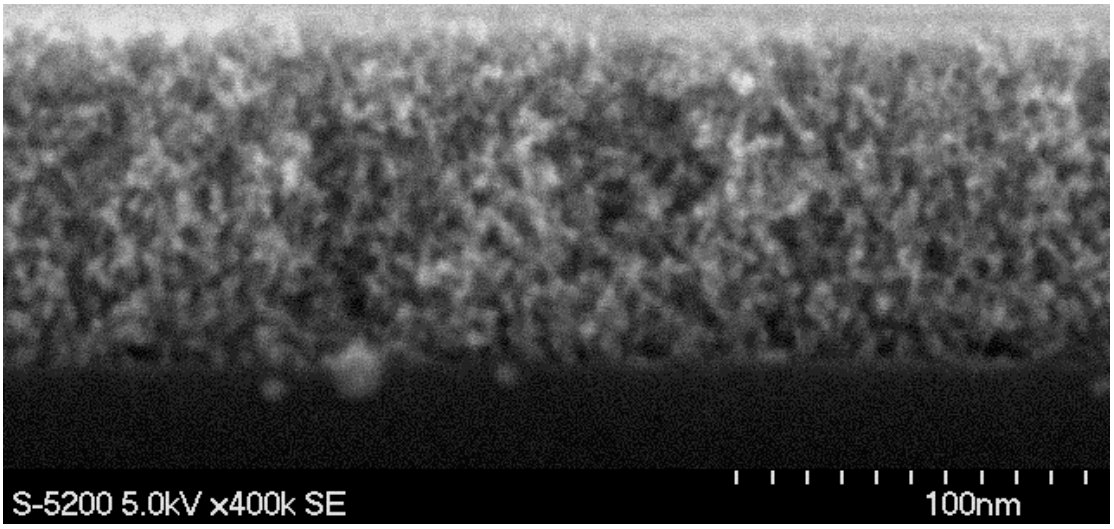

Figure S13: Example of a nanoporous ZTO (≡ SnO_2:Zn) thin film.

UV-Vis-NIR Spectra of TCO NPs:

The UV-Vis NIR spectra were recorded using TCO NP thin films, obtained by spin coating the dispersions over quartz slides and calcination under air at 450^{o}C for 15-20 mins. The spectra were recorded using a Perkin Elmer Lamda 900 spectrophotometer in transmittance mode with a scan speed of 125 nm/min. Spectra show that all the films are transparent in the visible region of the electromagnetic spectrum. The electronic band gap of each film was estimated from the spectra and shown in the insets. Notice the blue shift from the bulk band gap values which is in accordance with the particle size obtained from the PXRD data The spectra on the right hand side are the transmittance spectra of calcined samples. (Inserted is the calculated Tauc-Plot).

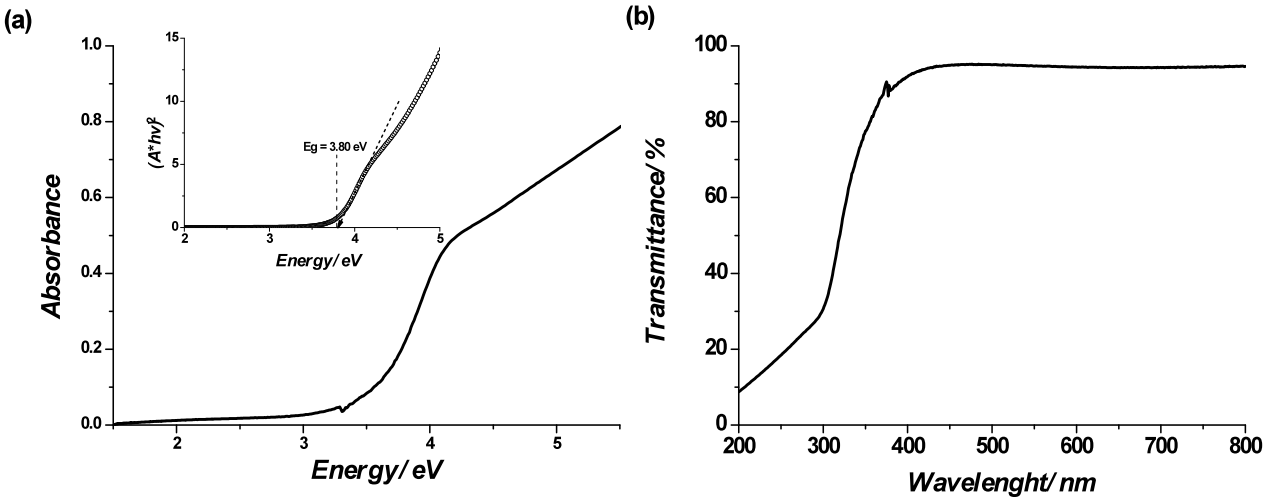

Figure S14. UV-Vis absorption spectrum (a) absorbance of fresh (I) and calcined at 450 ^{o}C (II) and (b) transmittance of calcined of In_2O_3. Inset in panel (a) is the Tauc plot of the calcined sample.

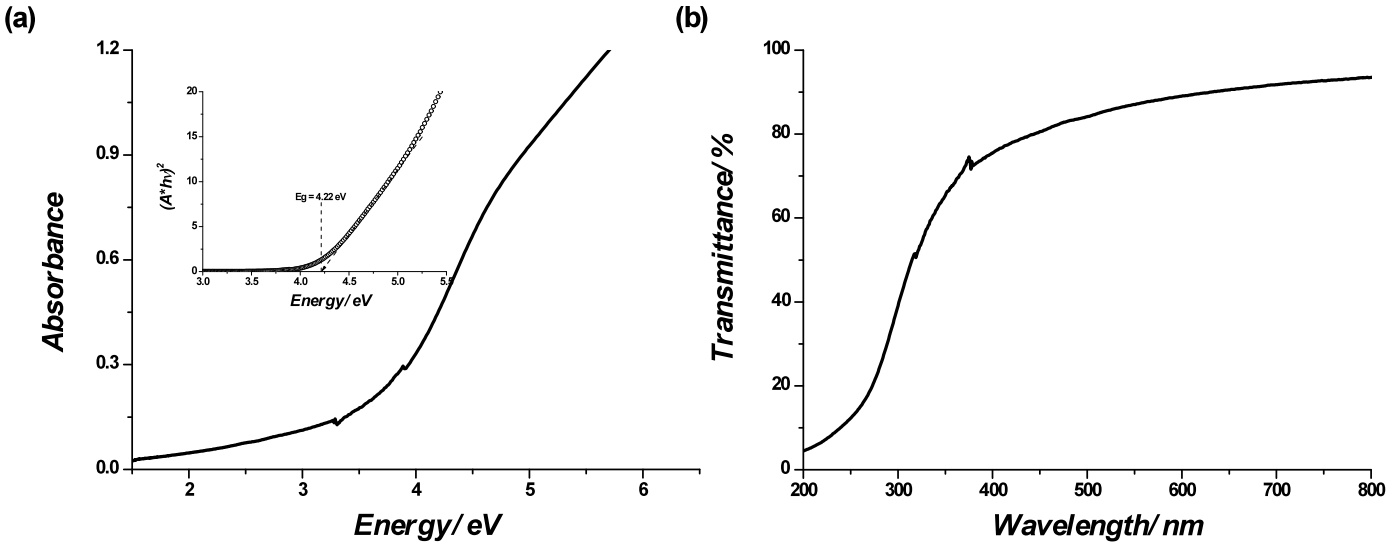

Figure S15. UV-Vis absorption (a) and transmittance (b) spectrum of NP SnO_2 calcined at 450^{o}C.

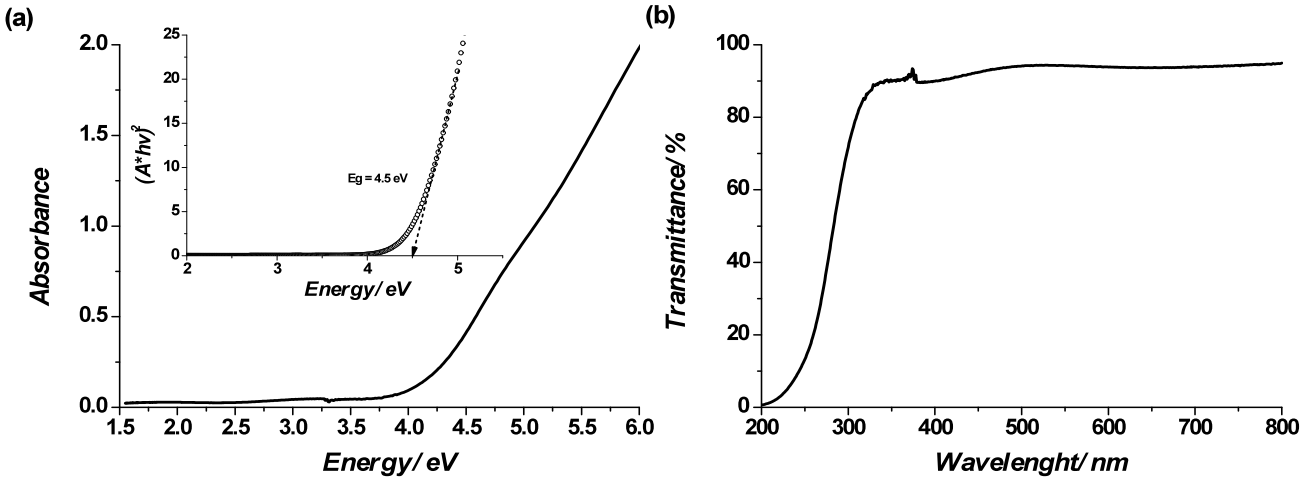

Figure S16. UV-Vis absorption (a) and transmittance (b) spectrum of NP ZTO calcined at 450^{o}C.

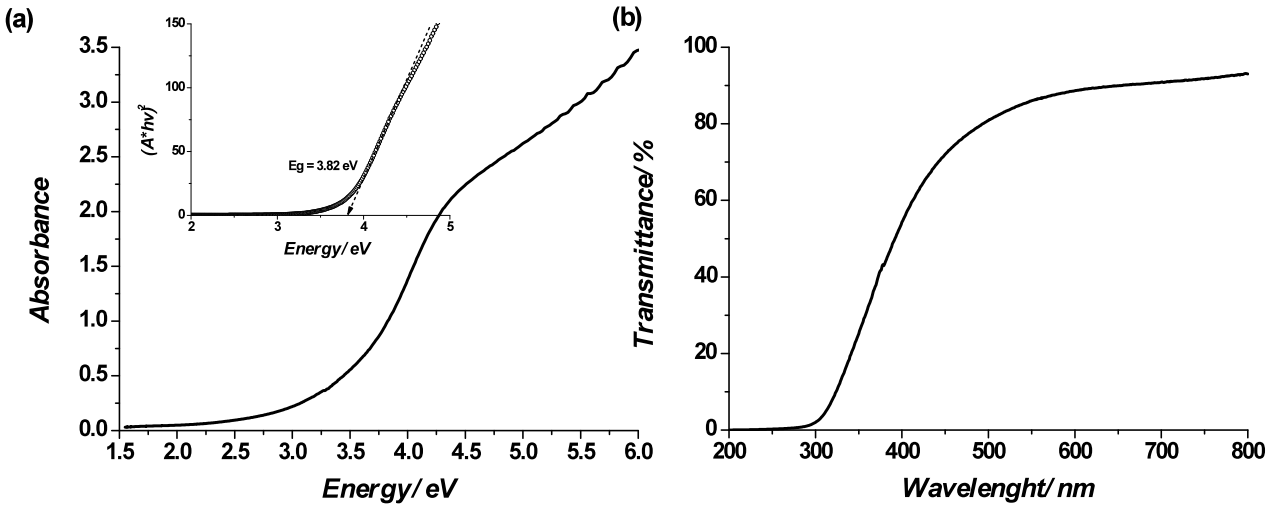

Figure S17. UV-Vis absorption (a) and transmittance (b) spectrum of NP ITO calcined at 450°C.

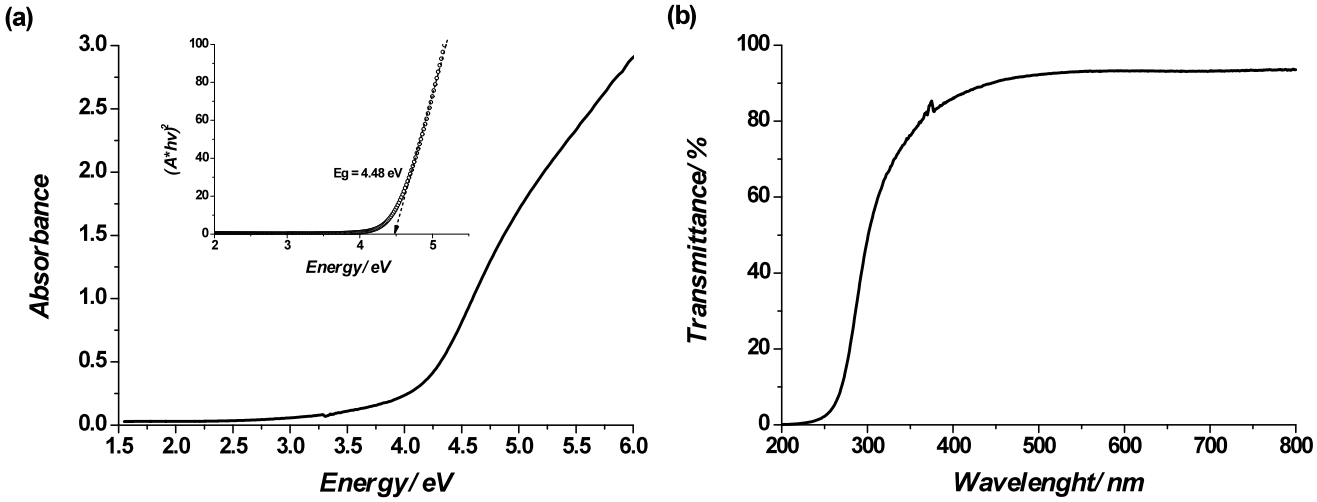

Figure S18. UV-Vis absorption (a) and transmittance (b) spectrum of NP ATO calcined at 450°C.

Table S3: Electronic band gaps (eV) of the calcined TCO NP films and bulk material for comparison in parenthesis

	Bad Gap (eV)
In_2O_3	3.80 (3.55-3.75)
SnO_2	4.22 (3.60)
ITO	3.82 (3.60)
ATO	4.48 (>3.60)
ZTO	4.50 (3.3-3.9)

Raman Spectroscopy of TCO NPs:

Micro-Raman spectra were recorded on a LabRam confocal Raman microscope with a 300 mm focal length. The spectrometer is equipped with a Ventus LP 532 50 mW, diode-pumped solid-state laser operated at 20 mW, with a polarization ratio of 100:1 and a wavelength of a 532.1 nm and a 1024x256 element CCD camera. The signal collected was transmitted via a fiber optic cable into a spectrometer with a 600 grazes/mm grating. The calcined samples typically show the spectra of corresponding oxide (Figures S19-S23, Table S4), but the dried samples (80°C under air) melts under the beam and/or under ambient conditions. There is a distinct difference between the calcined and just dried samples the origin of which is not clear.

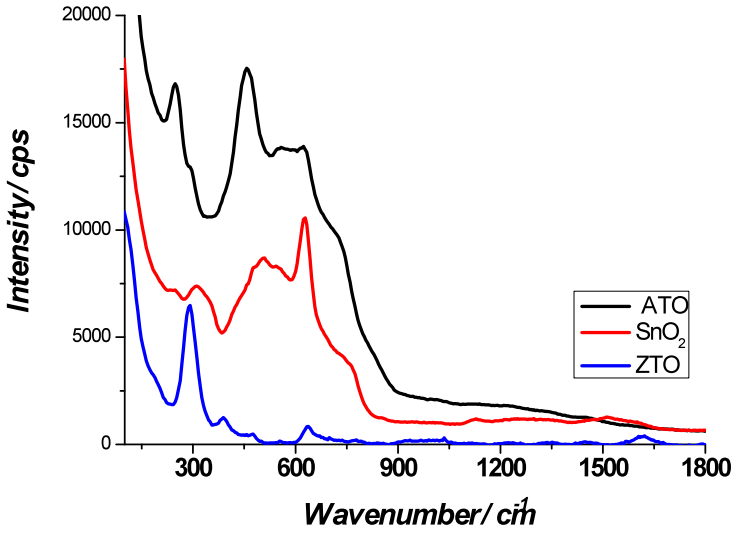

Figure S19. Raman spectra of ATO, SnO_2 and ZTO NP calcined at 450°C .

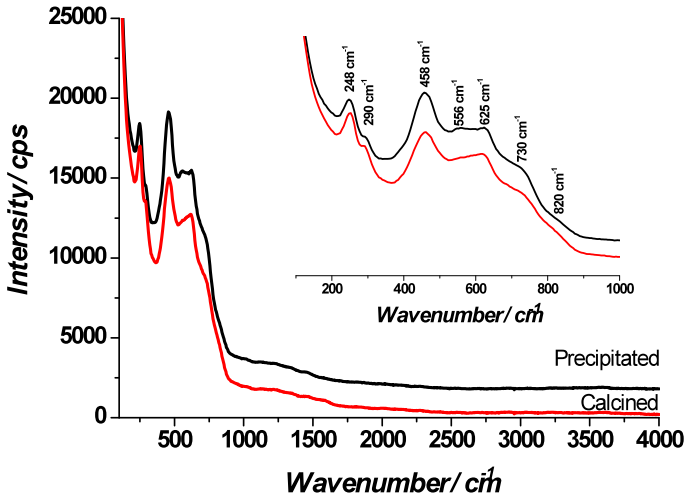

Figure S20. Raman spectra of ATO NP calcined at 450°C compared to the dried ATO NPs.

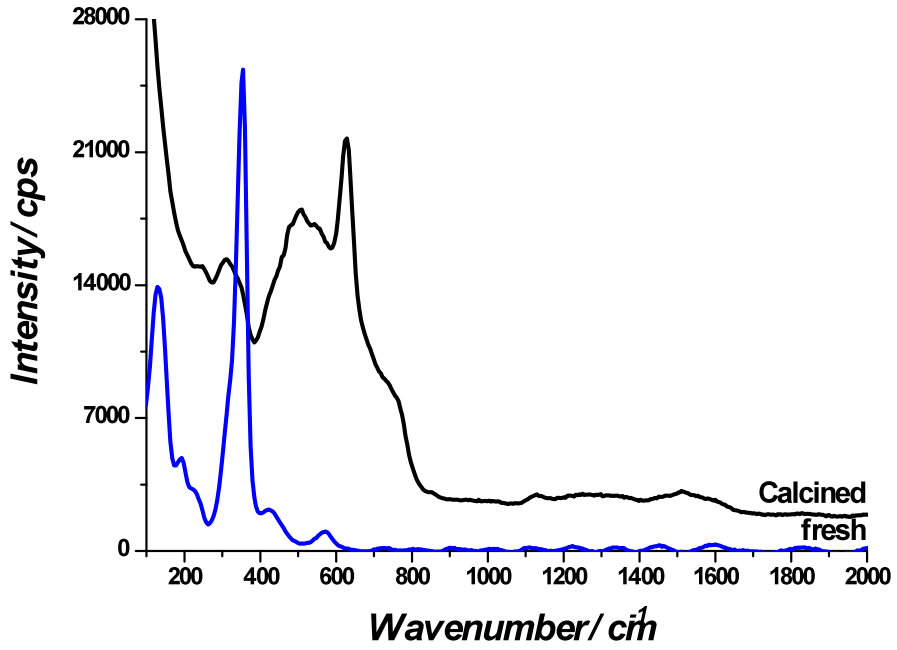

Figure S21. Raman spectra of SnO_2 calcined at 450 ^oC compared to dried (labeled fresh). The calcined samples display peaks due to Rutile SnO_2 at 313, 470, 620, 690, 770 cm^{-1}. The fresh sample displays peaks at 132, 195, 230, 315, 352, 424, and 572 cm^{-1}. The peaks at 132, 195, and 230 cm^{-1} corresponds to tin chloride surface species. (Ref. 1) A. Dieguez, A. Romano-Rodrigues, A. Vila, J. R. Morante, *J. Appl. Phys.* **2001**, *90*, 1550-1557. 2) M. Ristic, M. Ivanda, S. Popovic, S. Music, *J. Non-Crystal. Solids* **2002**, *303*, 270-280. 3) E. J. Hathaway, V. A. Maroni, *J. Phys. Chem.* **1972**, *76*, 2796-2798).

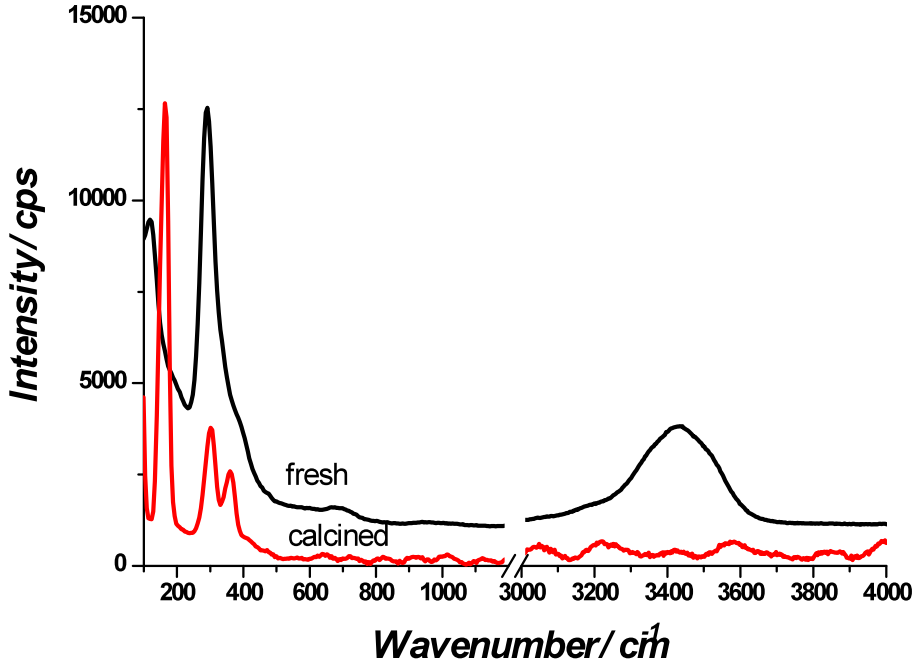

Figure S22. Raman spectra of In_2O_3 calcined at 450^oC compared to dried sample (labelled fresh). The indium dried sample shows a sharp peak at 90 and 290 cm^{-1} due respectively to δ-InCl and ν-In-Cl surface species. The other weak peaks at, 137, 308, 365, 504, 590 and 637 cm^{-1} are due to In_2O_3. (Ref, 1) W. B. White, V. G. Keramidas, *Spectrochemica Acta* **1972**, *28A*, 501-509. 2) D. Liu, W. W. Lei, B. Zou, S. D. Yu, J. Hao, K. Wang, B. B. Liu, Q. L. Cui, G. T. Zou, *J. Appl. Phys.* **2008**, *104*, 083506. 3) J. H. R. Clarke, R. E. Hester, *J. Chem. Phys.* **1969**, *50*, 3106-3112). Calcination removes most indium chloride surface species.

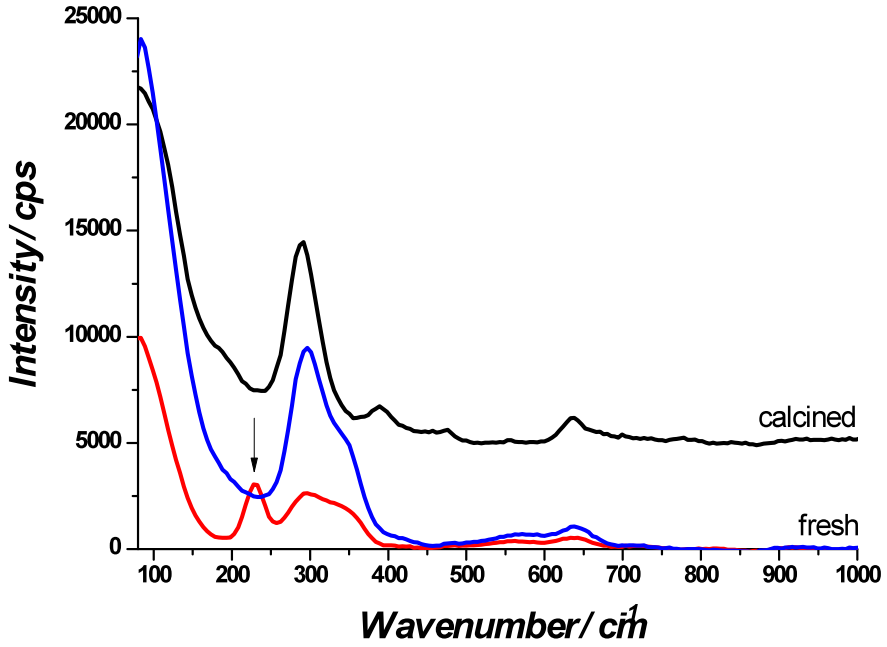

Figure S23. Raman spectra of ZTO NP calcined at 450°C and dried ZTO NP under the laser beam (labelled fresh, red spectrum is recorded first and the blue after exposure to laser beam).

Table S4: Raman frequencies of the as-synthesized dried and calcined In_2O_3, SnO_2, and mixed oxides ZTO, and ATO with tentative assignments.

Dried[a]			Calcined[b]			
In_2O_3 (cm^{-1})	**SnO_2 (cm^{-1})**	**ZTO (cm^{-1})**	**In_2O_3 (cm^{-1})**	**SnO_2 (cm^{-1})**	**ZTO (cm^{-1})**	**ATO[c] (cm^{-1})**
90 (δ-InCl)	132 (δ-SnCl)	230	90 (δ-InCl)			
117	195		164		178	
290 (ν-InCl and In_2O_3)	230 (ν-SnCl)	296	302	313 (ν-SnCl)	289, 340	248, 290
386	315		362	470 (E_g)	476	458
474	362	346		-	553	556
553	424	572		620 (A_{1g})	636	626
689	572			690 (LO or surface oxides)	-	730
		638		770 (B_{2g})	-	820

[a]The peaks due to surface species (M-Cl and peroxides) dominate in the dried samples, weak peaks in the 1000-1600 cm^{-1} region are due to peroxy surface species. [b]Raman active peaks are slightly red shifted from bulk Rutile SnO_2. Common peaks (slightly shifted from SnO_2) in the calcined ZTO and ATO samples belong to SnO_2. High frequency peaks are surface oxides. [c]Dried and calcined ATO have very similar spectra.

Zeta Potential and Dynamic Light Scattering Measurements of TCO NPs:

Electrophoretic mobility measurements and dynamic light scattering measurements at λ=633 nm were performed on ZetaSizer Nano-ZS, Malvern Instruments. Prior to analysis, the respective TCO NP samples were diluted with deionised H_2O in the ratio of 1:30 (pH ≡ 1.3 to 1.6) to obtain optical transparency for the DLS measurements. pH measurements were performed on a VWR SympHony SB70P laboratory pH meter. Additionally filtration through a 0.45 µm Nylon syringe-filter was performed to prepare a dust-free solution. A zeta potential transfer standard DTS 1230 (-68 ± 6.8 mV) was tested before measuring the samples. Nanoparticle zeta potential measurements (ζ) were performed by using a disposal Dipping Cell and repeated five times on each sample, for consistency purposes. The zeta potential measurements for the TCO nanoparticle diluted dispersions (1:30), at pH ≈ 1.3-1.7 have been found to be positive (e.g. ζ = 41.7 ± 1 mV for SnO_2, 26.1 ± 1.7 mV for ATO (≡ SnO_2:Sb) and 23.5 ± 1.4 mV for ZTO).

To determine the average particle size and particle size distribution by DLS measurements, for each sample, 11 single runs were measured. For statistical purpose 5 to 7 of these single runs are used to determine the average particle size and particle size distribution, see Examples **Figure S24 and S25** and **Table 1**.

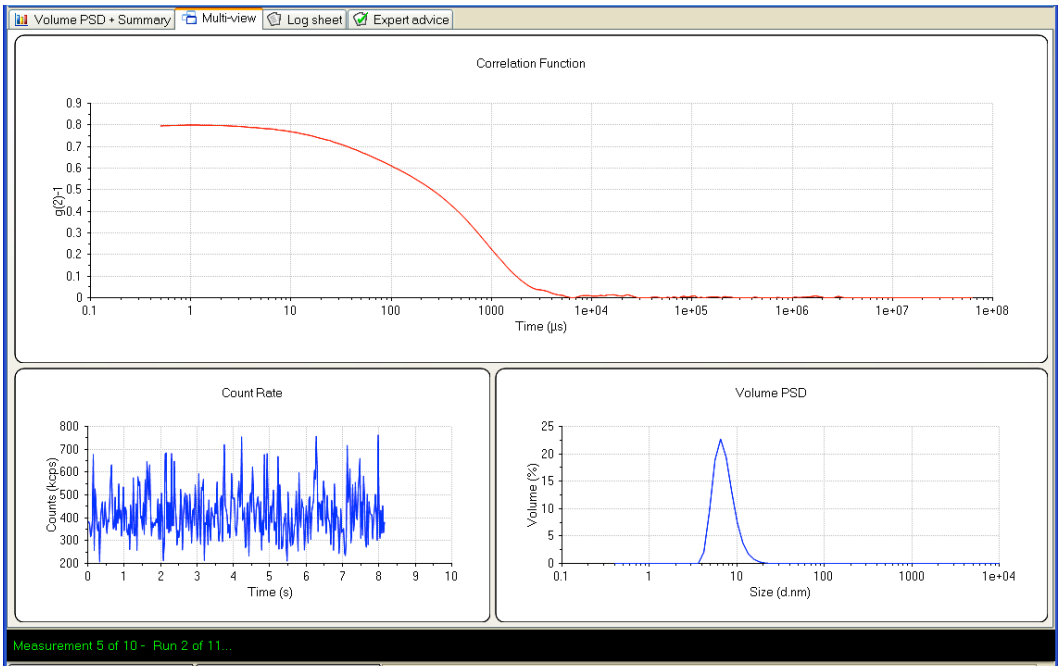

Figure S24. Example of a DLS measurement of a diluted (1:30) TCO NP sample

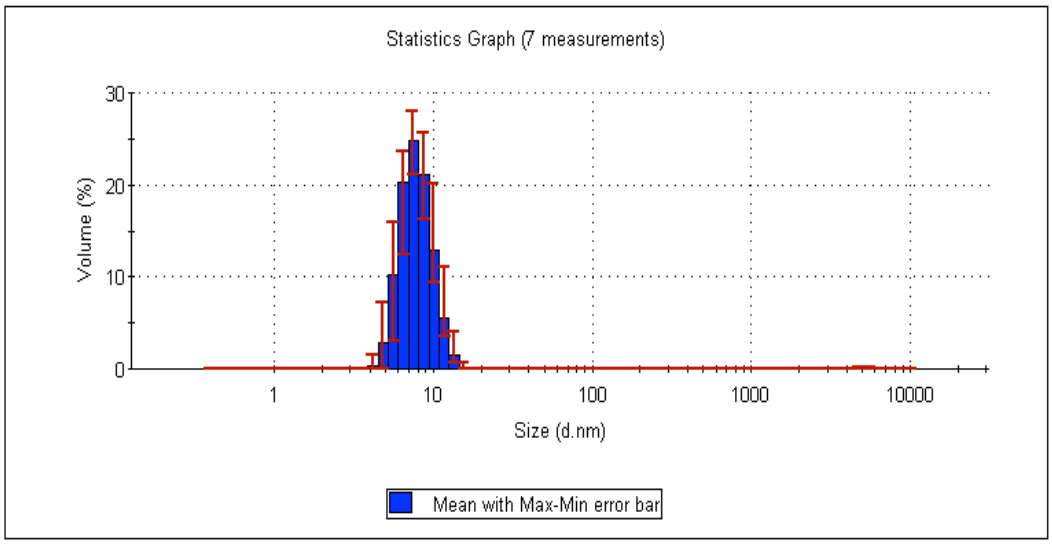

Figure S25. Example for DLS particle size distribution of the diluted SnO_2 dispersion 7.7 ± 1.6 nm

X-ray photoelectron spectroscopy (XPS) measurements:

XPS measurements were performed using a PHI 55000 Multi-Technique System using monochromatic Al Kα (hν = 1486.7 eV).

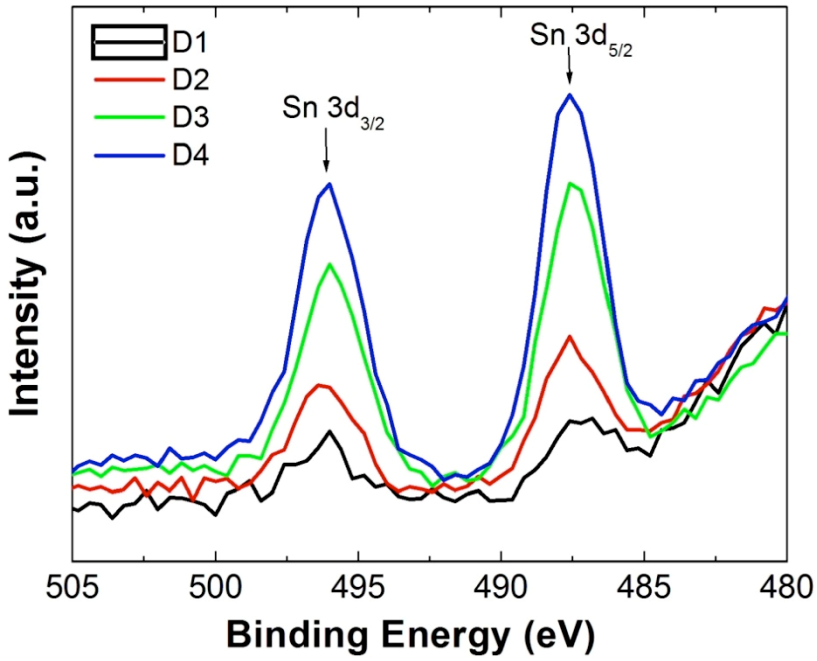

Figure S26. XPS data for increasing Sn doping levels in ITO NP (D1 to D4) samples: binding energy for Sn 3d5/2 is 487.5 eV, which matches Sn(IV) and is a n-dopant, for further reference see also: J. Luo, C. Xu, *Journal of Non-Crystalline Solids*, **1990**, *119*, 37-40.

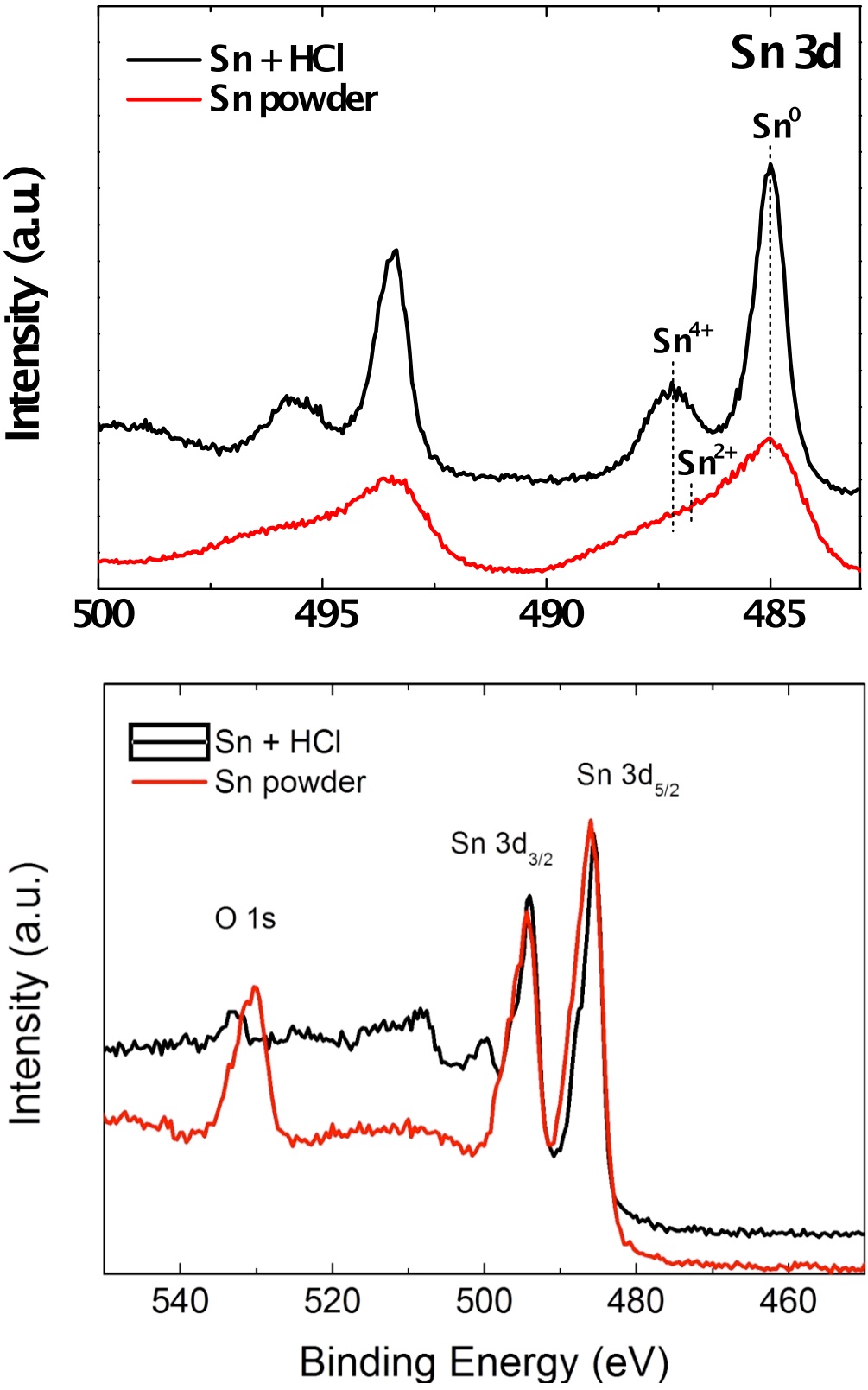

Figure S27. XPS data of the native Sn powder and the HCl treated/etched Sn powder. Etching of the native metal oxide (SnO_2) of bare Sn metal -powder clearly shows a significant lowering of the intensity of the O1s level after HCl treatment, as well a significant increase of the bare Sn(0) surface species.

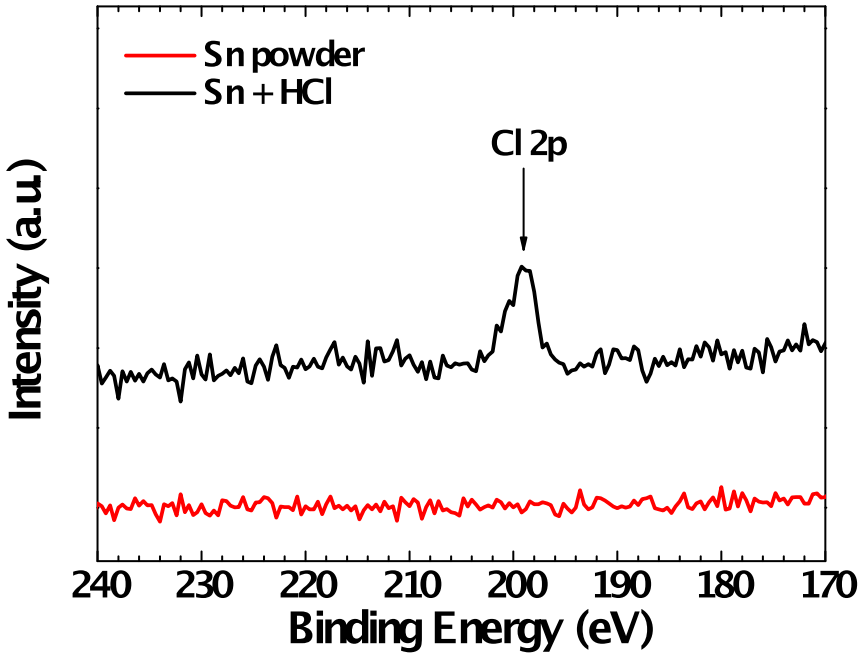

Figure S28. A weak Cl 2p signal can be observed after HCl treatment, which is consistent with our model that Cl^- species are absorbed the surface of the etched bare metal powder.

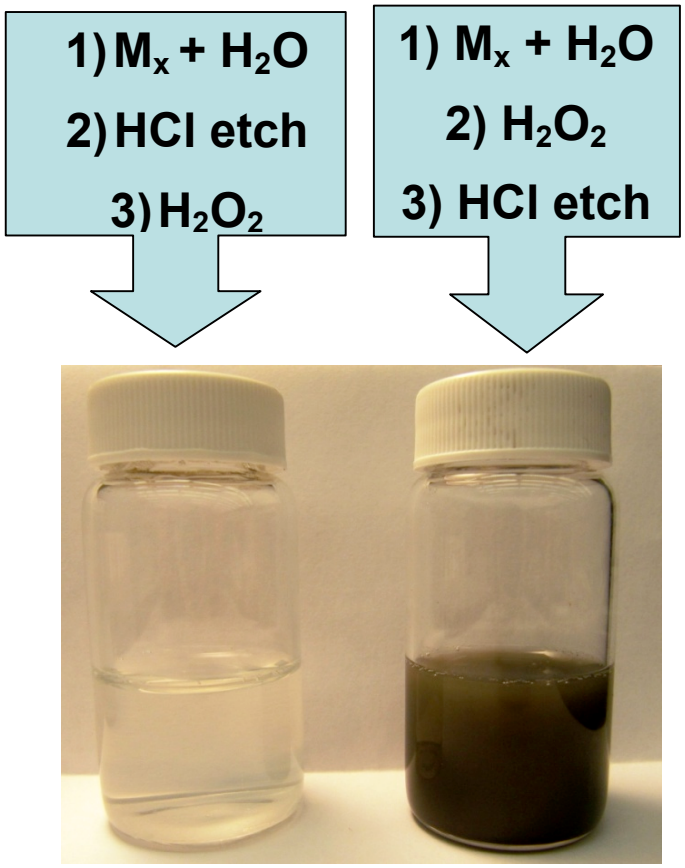

Figure S29. Key etching/treatment steps for the synthesis of TCO NP dispersions after 18h of stirring.

Resistivity Measurements:

The thicknesses of all samples used for resistivity measurements, estimated from cross-sectional SEM images, are ~100nm. Multiplying the sheet resistance by the thickness of the samples provides an estimate of the resistivity of the TCO NP films, which are shown in **Tables S5** and **S6**.

Table S5: Estimate of resistivity for TCO NP films annealed at different temperatures

NP Film	Resistivity [Ω·cm]	
	Annealed at 450°C	Annealed at 650°C
ATO	1.5×10^{1}	4.0
ITO	6.8	4.8
SnO_2	1.3×10^{3}	8.8×10^{2}
In_2O_3	5.6×10^{1}	3.7

Table S6: Estimate of resistivity for In_2O_3:Sn NP films annealed at different temperatures

NP Film	Resistivity [Ω·cm]	
	Before Annealing	After Annealing at 650°C
In_2O_3:Sn [5 wt% Sn]	1.3×10^{-1}	6.6×10^{-2}
In_2O_3:Sn [10 wt% Sn]	5.4×10^{-2}	1.9×10^{-2}
In_2O_3:Sn [15 wt% Sn]	5.5×10^{-2}	3.1×10^{-2}
In_2O_3:Sn [20 wt% Sn]	4.3×10^{-2}	3.1×10^{-2}